The Sr isotope geochemistry of oceanic ultramafic-hosted mineralizations

F. Hochscheid, Rémi Coltat, M. Ulrich, M. Munoz, G. Manatschal, Philippe Boulvais

Journal Pre-proofs

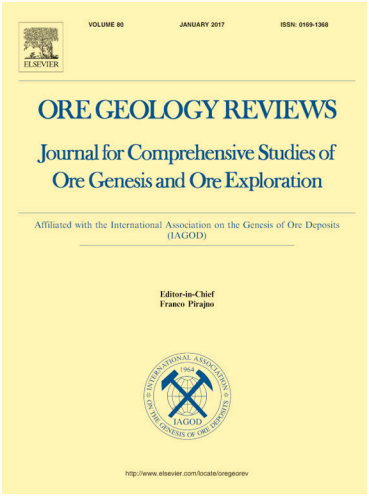

Review

The Sr isotope geochemistry of oceanic ultramafic-hosted mineralizations

F. Hochscheid, R. Coltat, M. Ulrich, M. Munoz, G. Manatschal, P. Boulvais

PII: S0169-1368(22)00132-9
DOI: https://doi.org/10.1016/j.oregeorev.2022.104824
Reference: OREGEO 104824

To appear in: *Ore Geology Reviews*

Received Date: 23 July 2021
Accepted Date: 6 March 2022

Please cite this article as: F. Hochscheid, R. Coltat, M. Ulrich, M. Munoz, G. Manatschal, P. Boulvais, The Sr isotope geochemistry of oceanic ultramafic-hosted mineralizations, *Ore Geology Reviews* (2022), doi: https://doi.org/10.1016/j.oregeorev.2022.104824

The Sr isotope geochemistry of oceanic ultramafic-hosted mineralizations

F. Hochscheid[a,*], R. Coltat[b], M. Ulrich[a], M. Munoz[c], G. Manatschal[a], P. Boulvais[b]

[a] *Institut Terre et Environnement de Strasbourg, Université de Strasbourg, EOST, CNRS UMR 7063, 5 rue Descartes, F-67084 Strasbourg*
[b] *Géosciences Rennes, Université de Rennes 1, CNRS UMR 6118, Campus Beaulieu, F-35000 Rennes*
[c] *Géosciences Montpellier, Université de Montpellier, CNRS UMR 5243, Campus Triolet, F-34095Montpellier*

Abstract

The source of metals involved in the formation of oceanic ultramafic-hosted hydrothermal Cu-Fe-Co-Zn-Ni mineralization remains poorly constrained. Here, we focus on a fossil ultramafic-hosted hydrothermal mineralized system preserved in the Platta nappe (SE Switzerland), where mantle rocks were exhumed along detachment faults to the seafloor during Jurassic rifting. The Cu-Fe-Co-Zn-Ni mineralization, associated with Fe-Ca-metasomatism (ilvaite-hydroandradite-diopside), represents an analogue of the root zone of present-day hydrothermal systems formed at mid-ocean ridges (e.g., Rainbow hydrothermal field at the Mid-Atlantic Ridge). We apply the Sr isotope geochemistry to Fe-Ca silicates and secondary, alteration products that include serpentinites, altered mafic and carbonated rocks to constrain the source(s) of metals and to characterize the plumbing system. The Fe-Ca silicates and carbonates have Sr isotope ratios close to that of Jurassic seawater, suggesting a near seafloor, seawater-dominated hydrothermal system with high fluid/rock ratios. The altered mafic rocks have $^{87}Sr/^{86}Sr$ ratios lower than those of Jurassic seawater. In contrast, serpentinites display a large range of Sr isotope ratios, including values higher than those of Jurassic seawater, indicating long lived fluid/rock interactions and

*Corresponding author, *Email address :* *fhochscheid@unistra.fr*

multi-stage fluid infiltrations. These results suggest that hydrothermal activity started during final crustal thinning, when seawater percolated along normal faults through the hyper-thinned crust, acquiring high Sr isotope ratios before penetrating and initiating serpentinization of the subcontinental mantle rocks. At this early stage, the system was rock-dominated (i.e., low fluid/rock ratios), leading to high $^{87}Sr/^{86}Sr$ ratios in serpentinites. On their way-back to seafloor, the uprising, serpentinization-derived fluids mixed with seawater resulting in the precipitation of metal sulfides and Fe-Ca silicates, with subsequent carbonation in a fluid-dominated system. Our study shows that the Sr isotope geochemistry can be used to identify reservoirs involved in the formation of mineral deposits and for the characterization of the plumbing system of oceanic ultramafic-hosted mineralizations.

Key words: Ultramafic-hosted metal deposits, Sr isotope geochemistry, Hydrothermal alteration, Ocean-Continent Transition, Alps, template

1. Introduction

Seawater circulation through the oceanic lithosphere plays a key role in heat and element transfers between the main Earth reservoirs, such as the mantle and seawater (Wolery and Sleep (1976); Bonatti et al. (1984); Alt (1995); Allen and Seyfried Jr (2004); Seyfried Jr et al. (2015) Humphris and Klein (2018); Le Gal et al. (2018)). During final rifting and breakup, extensional tectonics leads to the formation of high-angle normal and exhumation faults, which create preferential pathways for fluid circulation (Jackson (1987)). While hydrothermal fluids flow along these faults, they interact with the surrounding rocks, forming a variety of secondary rocks such as serpentinites, altered mafic rocks (among which rodingites) and ophicalcites (Spooner et al. (1974)). These alteration processes occur under a wide range of temperature, pH and redox conditions, leading to the formation of hydrothermal fluids with various chemical compositions (e.g., Früh-Green et al. (1990); Von Damm (1995); Seyfried Jr et al. (2004); Bach et al. (2004)). Among them, moderate to high-temperature, acidic and

reduced fluids are responsible for the formation of mineralized systems at or near the seafloor (Rona (1984); Rona et al. (1993); Hannington et al. (2001); Douville et al. (2002)). The discovery of ultramafic-hosted hydrothermal systems along slow- to ultra-slow-spreading ridges (Krasnov (1995); Fouquet et al. (1998); Cherkashov et al. (2008); Melchert et al. (2008); Tao et al. (2014); Tao et al. (2020)) or fossil systems in ophiolites preserved in the Alps (Garuti et al. (2008); Toffolo et al. (2017); Coltat et al. (2019b)) highlighted that hydrated ultramafic rocks may be suitable sinks for metals. In these geological settings, mineralization is commonly enriched in base (Cu, Zn, Ni), critical (Co), and precious metals (Au and Ag, Fouquet et al. (2013)).

Although our understanding of the formation of ultramafic-hosted hydrothermal systems has improved these last years, the source of metals in the mineralization is not fully constrained yet. Iron, Zn and Cu stable isotope systematics may bring constraints to decipher the source of metals and offer an interesting way of tracing metal mobilities in hydrothermal cells (Rouxel et al. (2004b), Rouxel et al. (2004a); Debret et al. (2018)). However, multiple factors control isotopic fractionation in these systems, including temperature, oxidation-reduction, multi-step processes, preventing to obtain a straightforward interpretation from isotopic compositions solely (Zhu et al. (2002)). On the opposite, the strontium isotopes are not subject to significant mass-dependent isotopic fractionation. The Sr isotope systematics are thus likely easier to interpret especially as the main terrestrial reservoirs (mantle reservoirs, continental crust, seawater) have distinct and well-defined Sr isotope compositions. Whereas exchanges between these reservoirs using Sr isotopes have been widely investigated (e.g., Veizer and Compston (1974); Chapman and Spooner (1977); Mcculloch et al. (1980); Albarede et al. (1981); Burke et al. (1982); Bach and Humphris (1999); Boschi et al. (2008); Delacour et al. (2008); Augustin et al. (2012); Schwarzenbach et al. (2021)), their application to mineralized systems has not been considered so far.

In the Platta nappe, in the SE Swiss Alps, Coltat et al. (2019b) identified a Jurassic mineralized system hosted in serpentinites considered to represent

an analogue of the root zone of active hydrothermal systems at slow-spreading ridges. The precipitation of metal-bearing phases (sulfides and oxides) was contemporaneous with a Fe-Ca-metasomatism responsible for the precipitation of Fe-Ca silicates (i.e., ilvaite, hydroandradite, diopside, Coltat et al. (2019b)). Since Ca and Sr share close chemical properties, these Fe-Ca metasomatic assemblages represent suitable targets for a Sr isotope-based tracing. These assemblages may have recorded isotopic information related to the metal source(s) involved in the formation of seafloor metal ore deposits and its related plumbing system.

Following this idea, we have measured the Sr isotope compositions of the Fe-Ca silicates that act as Sr sink. We also analyzed the potential contributors (i.e., the metasomatic rocks) and we compiled data from the literature. We discuss the implications of our results for the overall understanding of the formation of mineralized systems and more generally of fluid/rock interactions that occur during detachment-related mantle exhumation in oceanic domains.

2. Geological setting

2.1. The Platta nappe

The Platta nappe is located in the Central Alps in Grisons, SE Switzerland (Figure 1A). It corresponds to a remnant of the Alpine Tethys Ocean-Continent Transition (OCT), which formed during late Middle Jurassic when Europe and Adria separated. The Platta nappe is composed by serpentinized peridotites, mafic rocks (including basalts and gabbros) and post-rift sediments (Dietrich (1969), Manatschal and Nievergelt (1997); Desmurs et al. (2002); Schaltegger et al. (2002); Epin et al. (2019)). The Platta nappe is subdivided into two Alpine units (Figure 1B, C). The Upper Platta Unit mainly consists of serpentinized peridotites that originally formed the inherited subcontinental mantle of the Adriatic distal margin (i.e., the Err domain Schaltegger et al. (2002); Müntener et al. (2004); Müntener et al. (2010); Picazo et al. (2016); Epin and Manatschal (2018)). The Lower Platta Unit, originally located further oceanward, consists

of a large serpentinized mantle domain locally intruded by Jurassic gabbros and covered by pillow lavas, pillow breccias and locally also lava flows (Desmurs et al. (2002); Amann et al. (2020)). Contrarily to the mantle rocks from the Upper Platta Unit that do not exhibit any syn-rift melt imprint, those from the Lower Platta Unit have been largely refertilized by melt percolation during final rifting and breakup (Müntener et al. (2004); Müntener et al. (2010)).

The Platta nappe is separated, along an Alpine thrust, from the nappe stack preserving remnants of the former distal Adriatic continental margin (e.g. Err and more proximal domains of the former Adriatic margin). Slivers of continental origin also occur in the Platta nappe and have been interpreted as extensional allochthons (Froitzheim and Manatschal (1996)). Based on this observation and the subcontinental nature of the mantle, the Platta nappe has been considered as a magma-poor OCT of late Middle Jurassic age (Froitzheim and Manatschal (1996); Manatschal and Nievergelt (1997); Figure 1). Mantle exhumation in the OCT was accommodated along multiple detachment faults (Epin et al. (2019)) accompanied with the inception of mafic magmatism. More detailed mapping enabled to propose the existence of a well preserved mantle core complex, capped by a main extensional detachment and overprinted by later high-angle faults Epin et al. (2019). U-Pb dating on zircons from syn-tectonic mafic intrusions provided a Jurassic age of 161 $\pm$1 Ma for the timing of mantle exhumation (Schaltegger et al. (2002)). This exhumation phase was accompanied by intense fluid circulations, leading to (i) serpentinization of ultramafic rocks, (ii) rodingitization of mafic intrusive and epidotization-chloritization of mafic extrusive rocks (Desmurs et al. (2002); Amann et al. (2020)), (iii) formation of mineralized systems (Dietrich et al. (1972); Perseil and Latouche (1989); Coltat et al. (2019b)) and (iv) carbonation of serpentinites and basalts near and at the seafloor along the exhumed detachment surface (Coltat et al. (2019a); Coltat et al. (2020)).

Reactivation of the Alpine Tethys margin during Alpine convergence can be subdivided into three stages. During a first Late Cretaceous phase (D1 of Froitzheim (1994), the whole Adriatic margin was telescoped along major, west-

verging thrusts during which the Platta nappe became part of the main Alpine nappe stack (Figure 1B, C). The second phase (D2) corresponds to a late Cretaceous extensional event forming top-to-the-east to top-to-the-southeast normal faults. This phase is followed by a third phase (D3) that produced east-west trending folds with steeply dipping axial planes and a few north-vergent folds and thrusts with minor displacement (some few meters at a maximum). It is worthy to note that the whole Platta Nappe has been relatively preserved from Alpine deformation (only D1 results in a main overprint) and the metamorphic overprint was week with maximum conditions corresponding to prehnite-pumpellyite metamorphism (less than 350°C) (see Coltat et al. (2021). It is also important to note that the Platta nappe remained in the hanging wall of the Late Cretaceous to Cenozoic subduction, which differs from most Alpine ophiolites exposed in the Western Alps. Therefore, the pre-Alpine seafloor-related structures and hydrothermal alterations remained largely preserved (Froitzheim and Manatschal (1996); Chalot-Prat et al. (2003); Epin et al. (2019)).

2.2. The Marmorera-Cotschen Hydrothermal System

A well-preserved fossil ultramafic-hosted hydrothermal system, namely the Marmorera-Cotschen hydrothermal system, has been recently identified in the Platta Nappe (Coltat et al. (2019b); Coltat et al. (2021)). This hydrothermal system is preserved in the serpentinized footwall of a detachment fault juxtaposing basalts onto serpentinites (Figure 1B, Coltat et al. (2019b)). The serpentinite-hosted mineralization is geometrically associated with mafic intrusions indicating that the latter acted as preferential pathways for the fluid. The Cu-Fe-Co-Zn-Ni mineralization consists of sulfides (mainly chalcopyrite, pyrrhotite, (Co-)pentlandite and sphalerite) and oxides (magnetite). Geochemical analyses performed on massive sulfides show enrichments up to 27.7 wt. % Cu, 0.28 wt. % Zn, 0.16 wt. % Co and Ni content of about ∼1500 ppm, similar to those of unaltered mantle rocks (Coltat et al. (2021)). Gold was never concentrated enough to be detected in Cu-rich massive sulfides but Ag concentration reach up to ∼120 ppm in the most mineralized samples (Coltat

et al. (2021)). A Fe-Ca-metasomatism responsible for the formation of Fe-Ca silicates such as ilvaite, hydroandradite and Fe-rich diopside as stockwork zones and pervasive replacement zones in serpentinites was coeval with the mineralization (Coltat et al. (2019b)). Based on petrographic and structural features, the Marmorera-Cotschen hydrothermal system is assumed to represent the root of an ultramafic-hosted black smoker system (Coltat et al. (2019b)).

3. Methods

3.1. Field sampling

In this study, we present the Sr isotope compositions of 64 samples from the Platta nappe including Fe-Ca silicate minerals (12 samples), carbonated rocks (15 samples), serpentinites (24 samples) and mafic rocks (8 samples). In order to unravel the hydrothermal alterations during the tectonic evolution of the margin, we collected samples at different structural positions along the margin, from the continentward (Upper Platta) to the oceanward (Marmorera-Cotschen, Lower Platta) domains (Table 1; Figure 1B, C). Several Sr sources are supposed to be involved for the considered hydrothermal alterations, such as the Jurassic seawater , the subcontinental lithospheric mantle and the continental crust.

The Fe-Ca silicate minerals were sampled at two different sites: Cotschen and Kanonensattel (i.e., the eastern prolongation of the Marmorera-Cotschen hydrothermal system, for location see Figure 1B). The site of Cotschen corresponds to the deepest structural position of the hydrothermal system and is located about 150 m below the detachment/seafloor. Based on mineralogical assemblages reported in the mineralization at Kanonensattel, this site also likely corresponds to a deep part of the hydrothermal system, although the contact between serpentinites and mafic rocks (i.e., the detachment surface) has not been observed. The potential variations of the fluid/rock interactions during Fe-Ca-metasomatism were tested by sampling both Fe-Ca silicate minerals in the stockwork zone (Figure 2A) and those that pervasively replaced the serpentinites (Figure 2B).

Carbonated rocks, especially marine carbonates are often used to determine the Sr isotope composition of seawater through geological times since they presumably precipitated at isotopic equilibrium with seawater (Burke et al. (1982)). In the Jurassic, the $^{87}Sr/^{86}Sr$ ratio of seawater is between 0.7068 and 0.7078 (DePaolo and Ingram (1985), Hess et al. (1986), McArthur et al. (1993), Jones et al. (1994), Veizer et al. (1999). In the Platta nappe, ophicalcites and carbonated mafic rocks from different sites (i.e. Cotschen, Marmorera, Falotta, Figure 1B; Table 1) were analyzed in order to better constrain the Sr isotope value of seawater when carbonation occurred. The sampled rocks include discrete calcite veins crosscutting the serpentinites (i.e. fracture infilling ophicalcites in Coltat et al. (2019a)) and mafic rocks (Figure 2C) as well as thick carbonated shear bands in serpentinites (i.e., foliated ophicalcites in Coltat et al. (2019a); Figure 2D). The latter are assumed to form under higher fluid/rock ratios than the former, making them suitable candidates to record the original $^{87}Sr/^{86}Sr$ value of seawater.

The Sr reservoirs implied in the serpentinization of mantle rocks can be deduced from the isotope compositions of serpentinites through the Platta nappe. The serpentinites display several generations of serpentine minerals, with a predominant one presenting a typical mesh texture (the groundmass), and a series of green veins crosscutting the mesh (Figure 2E; referred to as veins in Table 1). These two types of serpentinite are supposed to record different conditions of formation during mantle exhumation Picazo et al. (2013).

In addition to serpentinites and carbonates, eight mafic rocks, including epidotized and chloritized basalts (Figure 2F) and chlorite/actinolite-bearing mafic intrusions have been analyzed. Our geochemical dataset (Table 1) is completed by data from the literature for mafic rocks, rodingites and associated blackwalls of the Platta nappe (See supplementary material; Stille et al. (1989); Schaltegger et al. (2002) and Amann (2017)).

3.2. Analytical methods

The whole-rock analysis of serpentinites and mafic rocks was carried out to determine the Sr and Rb contents of the rocks. Trace elements were measured by Inductively Coupled Plasma Mass Spectrometry (ICP-MS; Thermo Scientic X series II instrument) at the Institut Terre et Environnement de Strasbourg (ITES). Following the analytical procedure of Chauvel et al. (2011), about 100 mg of rock powder was precisely weighed and dissolved in Savillex beakers in a HF-HNO_3-$HClO_4$ (5:1:1) mixture, during a minimum of 7 days at 140°C on a hot plate. The solution was then evaporated and the residue dissolved in concentrated HNO_3 and evaporated before dilution in about 40 ml of 7 M HNO_3.

The Sr isotope compositions of whole rock samples (serpentinites, mafic rocks, rodingites and blackwall) were determined at the Institut Terre et Environnement de Strasbourg (ITES) using a Neptune Thermo Scientific instrument Multi-Collector Inductively Coupled Plasma Mass Spectrometer (MC-ICP-MS) and a Thermo Finnigan Triton instrument Thermal Ionisation Mass Spectrometer (TIMS). About 100 mg of rock powder was dissolved and digested in a HF:HNO_3:$HClO_4$ (5:1:1) mixture for 7 days. The samples were then evaporated and the residues taken up in concentrated HNO_3 to ensure complete dissolution. After another evaporation, the samples were finally dissolved in 2ml of 2 M HNO_3 before being loaded in resin columns (Eichrom Sr-spec resin), washed with 5.5 ml of HNO_3 7 M and then eluted with 2.4 ml of HNO_3 0.05 M. Chemical separation and purification were performed following an analytical procedure modified after Pin and Zalduegui (1997) and Deniel and Pin (2001). Measured $^{87}Sr/^{86}Sr$ ratios were normalized to $^{86}Sr/^{88}Sr = 0.1194$. During the collection of isotopic data, replicate analysis of NBS 987 ($SrCO_3$) reference material gave a mean value of 0.710260 ± 8 (2 SE, n = 26). The total procedural blank for the whole chemical treatment was 207-233 pg, negligible for all samples.

The Sr isotope composition of carbonates were determined at Geosciences Rennes, Université de Rennes 1, using a Mat Finnigan 262 instrument (TIMS). Approximatively 10 mg of rock powder were sampled by micro drilling and then

dissolved in 2.5 M HCl before chemical separation.

The $^{87}Sr/^{86}Sr$ ratios for serpentinites, mafic rocks, rodingites and blackwalls were recalculated at 160 Ma, based on the age of magmatic intrusions and gabbros of the Platta nappe. For Fe-Ca silicates, Rb concentrations were systematically below the detection limit, and for carbonated rocks, it was presumed that the Rb content is extremely low, giving a Rb/Sr ratio close to zero; therefore it was assumed that the $^{87}Sr/^{86}Sr$ ratio of these samples did not significantly evolve during the last 160 Ma (Table 1).

4. Sr isotope compositions of altered rocks from the Platta nappe

4.1. Fe-Ca silicates in veins and pervasively replacing serpentinites

The Sr isotope ratios of Fe-Ca silicates range from 0.70592 to 0.70785 with an average composition close to the value of Jurassic seawater (∼0.7068, n = 12, Figure 3). At Kanonensattel, Fe-Ca silicates that pervasively replaced serpentine are more radiogenic than those from Cotschen (mean values of 0.70708 and 0.70648, respectively, Table 1). At Cotschen, Fe-Ca silicates occurring as pervasive replacement are slightly more radiogenic than those in veins crosscutting serpentinites (0.70676 and 0.70621, respectively Table 1).

4.2. Carbonates veins and shear bands in serpentinites and basalts

The $^{87}Sr/^{86}Sr$ ratios of carbonates are centered around 0.70668 (n = 15; Table 1), close to the value of Jurassic seawater (Figure 3). The carbonated rocks from Falotta display Sr isotope ratios comprised between 0.70624 and 0.70729, with a mean value of 0.70684, while carbonates from Cotschen are less radiogenic (0.70645 in average). Carbonates from Marmorera exhibit low Sr isotope ratios, with maximum at 0.70548. Carbonate veins in serpentinites show the highest variability of Sr isotope compositions, ranging from 0.70419 to 0.70729, with a mean value slightly below the Jurassic seawater (0.70640, Table 1). At Falotta, discrete carbonate veins in serpentinites display Sr isotope ratios higher than their equivalents in mafic rocks (0.70706 vs. 0.70665, respectively) or

than carbonated shear bands in serpentinites (0.70686; Table 1). At Marmorera, carbonates in pervasive replacement of serpentinites display lower Sr isotope ratios than calcite veins in serpentinites (0.70468 and 0.70484, respectively; Table 1).

4.3. Serpentinites

Serpentinites are characterized by $^{87}Sr/^{86}Sr$ ratios of 0.70394 to 0.7939, values that range between those of the sub-continental lithospheric mantle and the mean value of the continental crust (Figure 3). Numerous samples display Sr isotope ratios higher than the Jurassic seawater. As for carbonate veins, part of the isotope heterogeneity seems to be related to the structural position along the margin: serpentinites from the Upper Platta (proximal part of the paleo-margin) have higher $^{87}Sr/^{86}Sr$ ratios (0.70783 in average, n = 10) than those from the Lower Platta (0.70741, n = 14). In the latter, the less radiogenic sample is from Marmorera (0.70394), while serpentinites from Kanonensattel and Cotschen have similar and relatively high Sr isotope ratios (0.70717 in average; Table 1), close to the value of Jurassic seawater. In Falotta (Lower Platta), the Sr isotope ratios of serpentinites are more heterogenous, with a mean value of 0.70741 (n = 10; Table 1), higher than the Jurassic seawater. In addition, green serpentine veins (0.70832 in average) are characterized by higher Sr isotope compositions than serpentinites forming the groundmass (0.70717 in average).

4.4. Mafic rocks

The Sr isotope ratios of mafic rocks are consistent with those available in the literature (Stille et al. (1989); Schaltegger et al. (2002); Amann (2017); supplementary material). They range between the Jurassic seawater and the sub-continental lithospheric mantle (0.70181 to 0.70641; Figure 3). The mafic rocks from Marmorera ($^{87}Sr/^{86}Sr$=0.70400) have Sr isotope ratios lower than other samples from the Lower Platta (0.70603 in average), consistent with what is described for carbonates and serpentinites. Intrusive rocks display $^{87}Sr/^{86}Sr$ ratios lower than those for basalts (0.70351 and 0.70551 in average, respectively,

Table 1). Extrusive rocks display quite homogenous Sr isotope compositions regardless of their alteration (i.e., epidotization or chloritization), with a slightly less radiogenic composition for epidotized basalts when compared to chloritized basalts (0.70524 and 0.70606, respectively; Table 1).

4.5. Rodingites and blackwalls

Rodingites and blackwalls display $^{87}Sr/^{86}Sr$ ratios between 0.70345 and 0.70641 (see supplementary material online), overlapping those of mafic rocks (Figure 3). Rodingites display more radiogenic Sr compositions than blackwalls (0.70589, n = 6 and 0.70440, n = 4, respectively).

5. Discussion

5.1. Multiple Sr reservoirs involved during seafloor hydrothermalism in Ocean Continent Transition

Regardless the timing of the different hydrothermal alterations reported in the Platta nappe, the Sr isotope compositions of the altered rocks highlight that different Sr contributors were involved during hydrothermalism. The Sr isotope compositions of Fe-Ca silicates and carbonates are centered around the Jurassic seawater value (Figure 3). This suggests that seawater was the main contributor of strontium for these two lithologies, assuming that isotopic equilibrium was achieved. This is consistent with the development of ophicalcites within serpentinites close to the seafloor Weissert and Bernoulli (1984), and/or thanks to the infiltration of seawater during the syntectonic carbonation along the detachment fault and the serpentinite-basalt contact as evidenced by homogeneous stable $\delta^{18}O$ and $\delta^{13}C$ signatures of carbonates in the Falotta area (Coltat et al. (2019b)).

By contrast with other hydrothermal alteration products, many serpentinites display Sr isotope compositions significantly higher than the Jurassic seawater. This implies that the fluids responsible for serpentinization previously interacted with the continental crust, the latter reservoir being significantly more

radiogenic than Jurassic seawater (Figure 3). Hence, serpentinization of the sub-continental mantle occurred before its exhumation at the seafloor. A similar interpretation was proposed recently for serpentinization of mantle rocks in the Apennines Schwarzenbach et al. (2021).

The Sr isotope compositions of altered mafic rocks (i.e., epidotized and chloritized basalts) are slightly higher than those of fresh gabbros (Table 1). This observation can hardly be attributed to different magmatic parental sources since structural and geochemical relationships between intrusive and extrusive mafic rocks in the Platta nappe indicate they share a common genetic origin (Epin et al. (2019); Amann et al. (2020)). Consequently, we consider that the higher $^{87}Sr/^{86}Sr$ compositions of extrusive mafic rocks result from the interaction with seawater at higher fluid/rock ratios than for gabbros, which is similar to previous work (e.g., Burke et al. (1982);Rampone et al. (1998)). This inference is confirmed by the calculated percentage of Sr isotopic exchanged and fluid/rock ratios (Table 1). As the Jurassic seawater has a higher Sr isotope ratio than the sub-continental lithospheric mantle, intense alteration implying seawater circulation interacting with mafic rocks would ultimately lead to an increase of the Sr isotope compositions of the altered rocks.

As for mafic rocks, the Sr isotope compositions of rodingites and blackwalls range between the sub-continental lithospheric mantle value and that of Jurassic seawater (Figure 3), suggesting here again that the source of Sr predominantly derives from these two reservoirs during the hydrothermal alteration of mafic rocks. Rodingites and blackwalls have higher $^{87}Sr/^{86}Sr$ ratios than mafic rocks, which might also be explained by a more intense alteration highlighted by high Sr isotope exchange (supplementary materials). The involvement of modified seawater or different magmatic sources is an unlikely scenario that is discarded here. Indeed, in the rodingites from Falotta, which display the highest Sr isotope compositions (up to0.7068), primary minerals are completely replaced by secondary minerals (chlorite, grossular, diopside Amann (2017)). Besides, it is widely accepted that rodingites are formed by successive interactions between mafic rocks and fluids released after serpentinization reactions

(e.g., Coleman (1967); Frost (1975); Evans (1977); Palandri and Reed (2004); Panseri et al. (2008), Bach and Klein (2009); Salvioli-Mariani et al. (2020)). As shown earlier, some serpentinites have more radiogenic Sr isotope compositions than Jurassic seawater, especially at Falotta. Consequently, serpentinization-derived fluids reacting with mafic rocks would likely confer to rodingites and associated blackwalls higher Sr isotope compositions than those of the parental magmatic protolith.

5.2. Mineral textures as a proxy of fluid/rock ratios during hydrothermal alteration

The fluid/rock ratios prevailing during alteration can be calculated using the Sr isotope compositions of the altered rocks following the procedure describe in Delacour et al. (2008). Besides the isotopic variability explained by sourcing distinct reservoirs in variable amounts, some of the variability observed for a given lithology (dispersion of histograms; Figure 3) seems to be directly related to mineral textures, especially for Fe-Ca silicate minerals from Cotschen. The minerals in veins are less radiogenic than those in pervasive replacement of serpentinites (Table 1). This may relate to variable fluid/rock ratios and/or variable modes of secondary mineral formation during hydrothermal alteration (replacement vs. open-space infilling). This suggests close relationships between the replacement process and the resulting Sr isotope compositions. During hydrothermal alteration, the Sr isotope composition of secondary minerals is related to the amount of fluid available and its capacity to percolate into the rock. When large amounts of fluid are available (i.e., high fluid/rock ratio), the Sr isotope composition of the fluid remains unchanged during interaction with the country rocks and consequently, secondary minerals will record the isotopic signature of this fluid. On the contrary, if the amount of fluid available is low (i.e., low fluid/rock ratio), the initial Sr isotope composition of the fluid is modified during fluid/rock interactions and thus secondary minerals will record these fluid/rock interactions.

In cases where a large quantity of seawater was available, pervasive replace-

ment of primary minerals occurred, and the resulting Sr isotope compositions of altered rocks are close to the value of seawater (Figure 3). The initial Sr isotope compositions of protoliths, i.e., serpentinites both for Fe-Ca silicate minerals and carbonates, were erased during intense interaction with Jurassic seawater.

Conversely, if small amounts of seawater were involved, discrete veins preferentially formed, yielding Sr isotope compositions which were not buffered by seawater but rather preserved the ones of the primary host rocks. For instance, at Cotschen, the Fe-Ca silicate minerals produced during pervasive replacement of serpentinites display Sr isotope compositions close to that of Jurassic seawater (∼0.70676) and very large Sr isotope exchange (from 84 to 100 %), whereas isolated Fe-Ca silicate veins in serpentinites have slightly lower Sr isotope compositions (∼0.70621) and lower Sr isotope exchange (from 75 to 87 %). This supports the hypothesis of Coltat et al. (2019b), who proposed that the fluid/rock ratio increased from the outer zone (i.e., host serpentinites) where discrete veining occurred in the stockwork to the inner zone (i.e., Cu-rich massive sulfides) where Fe-Ca silicate minerals pervasively replaced the serpentinites.

As for Fe-Ca silicates, the textural variability of the carbonates at Falotta seems to control the Sr isotope compositions of altered rocks. Coltat et al. (2019a) inferred that an infinite isotopic reservoir was available during the formation of thick foliated ophicalcites (∼10 m). Fracture-filling carbonates, which formed under lower fluid/rock ratios than those prevailing for foliated ophicalcites, have higher Sr isotope compositions than the latter (0.70706 and 0.70686, respectively; Table 1). The percentage of Sr exchange calculated is about 96 % for foliated ophicalcites. This supports the idea that the textural variability of altered rocks is controlled by variations of the fluid/rock ratio during hydrothermal alteration, leading to distinct Sr isotope compositions of the secondary minerals. Where the fluid/rock ratio was high, secondary minerals recorded the Sr isotope composition of the fluid solely (i.e., seawater), whereas at low fluid/rock ratio, they recorded interactions between the hydrothermal fluid and the surrounding rocks (i.e., acquiring intermediate Sr isotope compositions between those of the fluid and the surrounding rocks). Similarly, Schwarzenbach

et al. (2021) have measured Sr and stable isotopes in calcite veins in ophicalcites from Apennine ophiolites, and proposed that carbonation resulted from extensive seawater circulation.

A different trend is recorded by serpentinites. At Falotta, the serpentine veins are more radiogenic than the groundmass of serpentines with mesh texture (0.70898 and 0.70756, respectively; Table 1). Mesh formation requires very low fluid/rock ratios and supports a diffusion process in a roughly closed system (where the amount of fluid is limited; Viti and Mellini (1998); Evans (2004); Andreani et al. (2007)). In contrast, vein formation corresponds to higher fluid/rock ratios, especially during the latest vein formation in an open system near the seafloor Andreani et al. (2007). The serpentine veins were formed after interaction with seawater that previously percolated through the continental crust. The oxygen isotope compositions measured in late serpentine veins from the Platta nappe by Früh-Green et al. (1990), are consistent with interaction with metamorphic fluids channelized along discrete brittle fractures and at grain boundaries in a rock-dominated system. More recently, Schwarzenbach et al. (2021) proposed that hydrogen isotopes compositions measured in serpentinites from the Apennine ophiolites resulted of a seafloor process and interaction with an evolved seawater-derived fluid. In the absence of evidence of metamorphic overprint in the area and in line with our results, we argue that this latter explanation is the most plausible.

5.3. Hydrothermal alteration during the final rifting and breakup of the Platta nappe

Part of the isotopic variability in serpentinites cannot be explained by variations of the fluid/rock ratios nor by mineral textures, e.g., the wide disparities in the groundmass serpentinites between sites (Table 1). Serpentinites in a more continentward position (Upper Platta) have $^{87}Sr/^{86}Sr$ ratios higher than serpentinites from a more oceanward position (Lower Platta; Table 1). For mafic rocks, epidotized basalts from Marmorera (distal domain) are less radiogenic than those from Falotta (distal domain; Table 1). Moreover, at Falotta, epido-

tized basalts recorded a higher Sr isotope exchange and fluid/rock ratio than those at Marmorera (Table 1). Therefore, the contribution of the Sr reservoirs likely evolved with the position along the margin and thus a change in the nature and the proportion of the Sr contributors during the margin formation may be inferred.

Serpentinization of mantle rocks resulted from the interaction of the subcontinental lithospheric mantle with hydrothermal fluids (Table 1; Figure 3) that previously interacted with the continental crust. During rifting, the continental crust was progressively thinned due to the interplay between brittle detachment faulting in upper crustal level and ductile shearing in middle and lower crustal levels (Mohn et al. (2012)). Hence, before reacting with mantle rocks, seawater likely percolated through the permeable faults and interacted with crustal rocks (Incerpi et al. (2020)). In a later stage of rifting, shear zone allowed to thin the crust less than 10 km and completely brittle, enabling faults and fluids to penetrate across the residual thinned crust into the mantle initiating serpentinization. At a following stage, mantle was exhumed to the seafloor by in and out of sequence detachment systems, whereby domains near the crust experienced contamination by continent-derived Sr, while this contamination decreased oceanward. This led to the Sr isotope gradient observed in serpentinites with lower Sr isotope compositions oceanward. Hence, a significant part of the isotopic heterogeneity of serpentinites is likely due to long-term serpentinization reactions during extensional tectonics, from the hyperextension phase to the exhumation phase (i.e., creation of the distal domain).

To a lesser extent, the position along the margin may also have influenced the Sr isotope compositions of carbonated rocks. Indeed, samples from Falotta (Figure 1B) display higher Sr isotope compositions than carbonated rocks from the more oceanward Cotschen and Marmorera domains. This could be explained by higher Sr isotope compositions of the host rocks at Falotta than at Marmorera-Cotschen (i.e., serpentinites Table 1; Figure 3). Hence, during carbonation, at a given fluid/rock ratio, the seawater that would have interacted with serpentinites having higher Sr isotope ratios at Falotta than at Marmorera-Cotschen

likely formed carbonates with higher Sr isotope compositions at Falotta.

5.4. Timing of the hydrothermal alteration at the Marmorera-Cotschen Hydrothermal System

All the points discussed above allow to propose a timing for the hydrothermal alteration and formation of the Marmorera-Cotschen hydrothermal plumbing system (Figure 4). In the Platta nappe hydrothermal alteration story, the serpentinization of mantle rocks was the first event (Figure 4, stage1). It started during the hyperextension phase of the rifting, when the sub-continental lithospheric mantle was still capped by a thinned continental crust (less than 10 km thick), forming the highly radiogenic serpentinites (Figure 3; Table 1). Serpentinization continued after mantle rocks exhumation at the seafloor (i.e., formation of the Ocean Continent Transition after continental breakup), leading to the interaction between mantle rocks and isotopically pristine seawater that circulated along the detachment faults (Figure 4, stage 2).

Mantle exhumation was accompanied by the emplacement of mafic magmatism (Desmurs et al. (2002); Epin et al. (2019); Amann et al. (2020)). Extrusive rocks were emplaced onto an active exhumation fault and were further altered during hydrothermal circulations, leading to epidotization, chloritization and late carbonation at the serpentinite-basalt interface (Coltat et al. (2019a); Coltat et al. (2020)). Rodingitization and associated blackwalls formed synchronously to the serpentinization of mantle rocks, through a diffusional metasomatism process between serpentinized-derived fluids and mafic rocks, such as described in Bach and Klein (2009) (Figure 4, stage 2). Here again, the heterogenous Sr isotope compositions of rodingites and blackwalls are consistent with long-term fluid/rock interactions and multi-stage infiltration of fluids Salvioli-Mariani et al. (2020). The fluids released during the rodingitization of mafic rocks migrated upwards and likely interacted with serpentinization-derived fluids and isotopically unmodified seawater to form Fe-Ca silicate minerals and late carbonates (Figure 4, stage 3 and 4, respectively).

The Sr isotope compositions of Fe-Ca silicate minerals and carbonated rocks

are centered around the value of seawater, especially those at Cotschen (Figure 3). The homogeneity of Sr isotope ratios and the large Sr exchange suggest short-lived fluid circulations under high fluid/rock ratios. Based on oxygen isotope compositions of ophicalcites, a similar interpretation was proposed by Coltat et al. (2019a) at the Falotta site (Lower Platta Unit) and in the Apennine ophiolites Schwarzenbach et al. (2021). Consistently, in our model, carbonation of mafic rocks and serpentinites was the latest hydrothermal event in the story. It is assumed to have occurred in high-permeability zones like the basalt-serpentinites interface during the mixing between seawater and uprising hydrothermal fluids. Towards the seafloor, the seawater component became more predominant (Figure 4, stage 4).

5.5. Consequences for the formation of ultramafic-hosted metal deposits

The Sr isotope compositions of Fe-Ca silicates accompanying mineralization in the Platta nappe are consistent with a contribution from the surrounding magmatic rocks (altered mafic and ultramafic rocks) but also from seawater (Figure 4D). The latter was also involved in metal precipitation (e.g. Co, Cu, Ni, Zn), during mixing with the hydrothermal fluid, as proposed for the Rainbow hydrothermal field (Debret et al. (2018)) and the fossil Marmorera-Cotschen hydrothermal system (Coltat et al. (2021)). However, it is unlikely that metals derived from seawater itself, even considering large fluid/rock ratios, since seawater contains infinitesimal proportions of metals compared to the surrounding rocks (e.g., Fouquet et al. (2013) and references therein). Rather, we propose that the main part of the metal stock involved for the Marmorera-Cotschen hydrothermal system mineralization derived from the surrounding rocks (serpentinites and mafic rocks) with minor involvement of seawater.

Based on S and Pb isotope geochemistry of ultramafic-hosted mineralizations, a similar scenario was proposed to explain metal enrichments at oceanic hydrothermal systems (Zeng et al. (2017)). These authors indicate that the contribution of seawater-derived sulfur taking part to mineralized systems was less than 36 %, whereas on the basis of Pb isotope compositions it was argued

that lead solely derived from the surrounding magmatic rocks. In addition, Debret et al. (2018) recently investigated the Fe, Cu and Zn systematics of barren and mineralized rocks from the ultramafic-hosted Rainbow hydrothermal system (MAR). They showed that serpentinization of mantle rocks was responsible for metal leaching from the parental peridotite (e.g., decreasing of metal concentrations from peridotite to serpentinite). Mantle rocks may thus represent a major contributor for metals involved in the formation of ultramafic-hosted mineralized systems.

Finally, the results from the present study highlight that the formation of ultramafic-hosted mineralized systems depends on the availability of both mafic and ultramafic reservoirs to extract metals that form economic mineralization enriched in base (Cu, Ni, Zn), critical (Co) and precious (Au) metals, similar to what is observed in present-day systems (Fouquet et al. (2013)). Recently, a review of fossil ultramafic-hosted mineralized systems preserved on-land has been proposed (Patten et al. (2021)). The main results are that: i) these systems are not scarce but rather represent a self-standing sub-group of the so-called volcanogenic massive sulfides (VMS) deposits, ii) they form in complex tectonic environments preserved in the geological record (e.g., ocean-continent transition, mid-oceanic ridge, supra-subduction zone), iii) they present specific alteration and deformation features (i.e. associated with serpentinites, carbonated mantle rocks and talc-chlorite-tremolite schists along extensional structures generally at the contact between mantle rocks and overlying mafic and/or sedimentary rocks), and iv) according to the Zipf's law, many deposits are still undiscovered. Although a genetic model is still missing for ultramafic-hosted VMS deposits, in which the Marmorera-Cotschen hydrothermal system belongs, our study, focused on the Sr isotope systematics, demonstrates that mafic and ultramafic reservoirs are important components that control the formation of polymetallic deposits. Similar mineralized systems have been reported at the contact between mantle and sedimentary rocks (e.g., Bouvier et al. (1990); Peltonen et al. (2008)), implying that mafic rocks are not a prerequisite to produce ultramafic-hosted metal deposits. Further studies are needed to produce a proper genetic

model for ultramafic-hosted VMS, especially concerning their relationships with the different hydrothermal alterations and the seafloor-related extensional tectonics, but this model will likely be implemented by Sr isotope investigations.

6. Conclusions

In the Platta nappe, the Fe-Ca silicates ($^{87}Sr/^{86}Sr = 0.70668$) and associated mineral deposits (the Marmorera-Cotschen hydrothermal system, of late Middle Jurassic age) formed through intense leaching of surrounding mafic and ultramafic rocks during interactions with seawater ($^{87}Sr/^{86}Sr = 0.70628$, this value being estimated using the most carbonated serpentines, i.e., the foliated ophicalcites). The Sr isotope compositions and textural features of altered rocks allowed to reconstruct the timing of the hydrothermal alteration and formation of the Marmorera-Cotschen hydrothermal plumbing system. The Sr isotope compositions of serpentinites recorded multiple and long-time fluid/rock interactions. In particular, the involvement of seawater is demonstrated, both during early stage (hyperextension phase) for which it interacted with continental crust and during late exhumation stage (mantle exhumation at the seafloor) during which it mixed with serpentinization-derived fluids. Obviously, the involvement of seawater became dominant during serpentinization and carbonation near the paleo-seafloor. Mafic rocks also recorded multiple fluid histories, involving variable amounts of hydrothermal fluids, leading to a diversity of Sr isotope compositions (from 0.70334 to 0.70624). In contrast, the Fe-Ca silicates and the ophicalcites mostly recorded latest stages of fluid/rock interactions dominated by seawater under high fluid/rock ratios. Rather than giving a straightforward information on the source of the metals present in ultramafic-hosted oceanic deposits, the Sr systematics thus helps identify the reservoirs involved in the mineralization and constrain the plumbing system through which mineralization occurred.

Acknowledgments

Yannick Branquet (University of Rennes 1) helped a lot during field work. David Vilbert (Géosciences Rennes) and Clément Bujisho (Master 1 internship at the University of Rennes 1) performed the analyses on carbonates and some Fe-Ca silicates. Eric Pelt (ITES - University of Strasbourg) helped for isotopic measurements and René Boutin performed ICP-MS analyses. This work was supported by the French National program INSU-SYSTER and by the AAP interne of ITES.

References

References

Albarede F, Michard A, Minster JF, Michard G. 87sr/86sr ratios in hydrothermal waters and deposits from the east pacific rise at 21°N. Earth and Planetary Science Letters 1981;55:229–36.

Allen DE, Seyfried Jr W. Serpentinization and heat generation: constraints from Lost City and Rainbow hydrothermal systems. Geochimica et Cosmochimica Acta 2004;68(6):1347–54. doi:10.1016/j.gca.2003.09.003.

Alt JC. Subseafloor processes in mid-ocean ridge hydrothermal systems. Geophysical Monograph-American Geophysical Union 1995;91:85–.

Amann M. Evolution du magmatisme et du metasomatisme dans une marge passive pauvre en magma durant l'initiation de l'accretion oceanique: Exemple de la marge fossile de la platta (alpes suisses) et comparaison avec le systeme actuel iberie-terre neuve. 2017;.

Amann M, Ulrich M, Manatschal G, Pelt E, Epin ME, Autin J, Sauter D. Geochemical characteristics of basalts related to incipient oceanization: The example from the Alpine-Tethys OCTs. Terra Nova 2020;32:75–88. doi:10.1111/ter.12438.

Andreani M, Mevel C, Boullier AM, Escartin J. Dynamic control on serpentine crystallization in veins: Constraints on hydration processes in oceanic peridotites. Geochemistry, Geophysics, Geosystems 2007;8. doi:10.1029/2006GC001373.

Augustin N, Paulick H, Lackschewitz K, Eisenhauer A, Garbe-Schönberg D, Kuhn T, Botz R, Schmidt M. Alteration at the ultramafic-hosted logatchev hydrothermal field: Constraints from trace element and sr-o isotope data. Geochemistry, Geophysics, Geosystems 2012;13(3).

Bach W, Garrido CJ, Paulick H, Harvey J, Rosner M. Seawater-peridotite interactions: First insights from ODP leg 209, MAR 15°N. Geochemistry, Geophysics, Geosystems 2004;5. doi:10.1029/2004GC000744.

Bach W, Humphris SE. Relationship between the sr and o isotope compositions of hydrothermal fluids and the spreading and magma-supply rates at oceanic spreading centers. Geology 1999;27(12):1067–70.

Bach W, Klein F. The petrology of seafloor rodingites: insights from geochemical reaction path modeling. Lithos 2009;112(1-2):103–17. doi:10.1016/j.lithos.2008.10.022.

Bonatti E, Lawrence JR, Morandi N. Serpentinization of oceanic peridotites: temperature dependence of mineralogy and boron content. Earth and Planetary Science Letters 1984;70(1):88–94. doi:10.1016/0012-821X(84)90211-5.

Boschi C, Dini A, Früh-Green GL, Kelley DS. Isotopic and element exchange during serpentinization and metasomatism at the atlantis massif (mar 30 n): insights from b and sr isotope data. Geochimica et Cosmochimica Acta 2008;72(7):1801–23.

Bouvier JD, Dabrowski H, Jaffe FC, Vuagnat M. Le gisement cuprifère de saint-véran. Archives Des Sciences 1990;43:273–94.

Burke WH, Denison RE, Hetherington EA, Koepnick RB, Nelson HF, Otto JB. Geology variation of seawater 87sr/86sr throughout phanerozoic time

variation of seawater 87sr/86sr throughout phanerozoic time. The geology society of America 1982;10:516–9. doi:10.1130/0091-7613(1982)10<516.

Chalot-Prat F, Ganne J, Lombard A. No significant element transfer from the oceanic plate to the mantle wedge during subduction and exhumation of the Tethys lithosphere (Western Alps). Lithos 2003;69(3-4):69–103. doi:10.1016/S0024-4937(03)00047-1.

Chapman HJ, Spooner ETC. 87sr enrichment of ophiolitic sulphide deposits in cyprus confirms ore formation by circulating seawater. Earth and Planetary Science Letters 1977;35:71–8.

Chauvel C, Bureau S, Poggi C. Comprehensive chemical and isotopic analyses of basalt and sediment reference materials. Geostandards and Geoanalytical Research 2011;35(1):125–43.

Cherkashov G, Bel'tenev V, Ivanov V, Lazareva L, Samovarov M, Shilov V, Stepanova T, Glasby G, Kuznetsov V. Two new hydrothermal fields at the Mid-Atlantic Ridge. Marine Georesources and Geotechnology 2008;26(4):308–16. doi:10.1080/10641190802400708.

Coleman RG. Low-temperature reaction zones and Alpine ultramafic rocks of California, Oregon and Washington. Geological Survey Bulletin 1247 1967;:46.

Coltat R, Boulvais P, Branquet Y, Collot J, Epin ME, Manatschal G. Syntectonic carbonation during synmagmatic mantle exhumation at an ocean-continent transition. Geology 2019a;47:183–6. doi:10.1130/G45530.1.

Coltat R, Boulvais P, Riegler T, Pelleter E, Branquet Y. Element distribution in the root zone of ultramafic-hosted black smoker-like systems: Constraints from an Alpine analog. Chemical Geology 2021;559. doi:10.1016/j.chemgeo.2020.119916.

Coltat R, Branquet Y, Gautier P, Boulvais P, Manatschal G. The nature of the interface between basalts and serpentinized mantle in oceanic domains:

Insights from a geological section in the Alps. Tectonophysics 2020;797. doi:10.1016/j.tecto.2020.228646.

Coltat R, Branquet Y, Gautier P, Rodriguez HC, Poujol M, Pelleter E, McClenaghan S, Manatschal G, Boulvais P. Unravelling the root zone of ultramafic-hosted black smokers-like hydrothermalism from an Alpine analog. Terra Nova 2019b;31:549–61. doi:10.1111/ter.12427.

Debret B, Beunon H, Mattielli N, Andreani M, da Costa IR, Escartin J. Ore component mobility, transport and mineralization at mid-oceanic ridges: A stable isotopes (zn, cu and fe) study of the rainbow massif (mid-atlantic ridge 36°14N). Earth and Planetary Science Letters 2018;503:170–80. doi:10.1016/j.epsl.2018.09.009.

Delacour A, Früh-Green GL, Frank M, Gutjahr M, Kelley DS. Sr-and nd-isotope geochemistry of the atlantis massif (30 n, mar): implications for fluid fluxes and lithospheric heterogeneity. Chemical Geology 2008;254(1-2):19–35.

Deniel C, Pin C. Single-stage method for the simultaneous isolation of lead and strontium from silicate samples for isotopic measurements. Analytica Chimica Acta 2001;426:95–103. doi:10.1016/S0003-2670(00)01185-5.

DePaolo DJ, Ingram BL. High-resolution stratigraphy with strontium isotopes. Science 1985;227(4689):938–41.

Desmurs L, Müntener O, Manatschal G. Onset of magmatic accretion within a magma-poor rifted margin: a case study from the Platta ocean-continent transition, eastern Switzerland. Contributions to Mineralogy and Petrology 2002;144(3):365–82. doi:10.1007/s00410-002-0403-4.

Dietrich V, et al. Die sulfidischen vererzungen in den oberhalbsteiner serpentiniten 1972;.

Dietrich VJ. Die ophiolithe des oberhalbsteins (graubünden) und das ophiolithmaterial der ostschweizerischen molasseablagerungen: ein petrographischer vergleich 1969;.

Douville E, Charlou JL, Oelkers EH, Bienvenu P, Colon CFJ, Donval JP, Fouquet Y, Prieur D, Appriou P. The rainbow vent fluids (36°14N, MAR): the influence of ultramafic rocks and phase separation on trace metal content in Mid-Atlantic Ridge hydrothermal fluids. Chemical Geology 2002;184:37–48. doi:10.1016/S0009-2541(01)00351-5.

Epin ME, Manatschal G. Three-dimensional architecture, structural evolution, and role of inheritance controlling detachment faulting at a hyperextended distal margin: The example of the Err detachment system (SE Switzerland). Tectonics 2018;37(12):4494–514. doi:10.1029/2018TC005125.

Epin ME, Manatschal G, Amman M, Ribes C, Clausse A, Guffon T, Lescanne M. Polyphase tectono-magmatic evolution during mantle exhumation in an ultra-distal, magma-poor rift domain: example of the fossil Platta ophiolite, SE Switzerland. International Journal of Earth Sciences 2019;108:2443–67. doi:10.1007/s00531-019-01772-0.

Evans BW. Metamorphism of Alpine peridotite and serpentinite. Annual Review of Earth and Planetary Sciences 1977;5:397–447. doi:10.1146/annurev.ea.05.050177.002145.

Evans BW. The serpentinite multisystem revisited: chrysotile is metastable. International Geology Review 2004;46(6):479–506. doi:10.2747/0020-6814.46.6.479.

Fouquet Y, Barriga F, Charlou JL, Elderfield H, German C, Ondreas H, Parson L, Radford-Knoery J, Relvas J, Ribeiro A, et al. Flores diving cruise with nautile near the azores-first dives on the rainbow field: hydrothermal seawater/mantle interaction. InterRidge News 1998;7(1):24–8.

Fouquet Y, Cambon P, Etoubleau J, Charlou JL, Ondreas H, Barriga FJ, Cherkashov G, Semkova T, Poroshina I, Bohn M, Donval JP, Henry K, Murphy P, Rouxel O. Geodiversity of hydrothermal processes along the Mid-Atlantic Ridge and ultramafic-hosted mineralization: A new type of oceanic

cu-zn-co-au volcanogenic massive sulfide deposit. Geophysical Monograph Series 2013;188:321–67. doi:10.1029/2008GM000746.

Froitzheim N. Repeated change from crustal shortening to orogenparallel extension in the austroalpine units of graubunden. Eclogae Geol 1994;87:559–612.

Froitzheim N, Manatschal G. Kinematics of jurassic rifting, mantle exhumation, and passive-margin formation in the Alpineustroalpine and penninic nappes (eastern switzerland). Geological society of America bulletin 1996;108(9):1120–33.

Frost R. Contact metamorphism of serpentinite, chloritic blackwall and rodingite at Paddy-Go-Easy Pass, Central Cascades, washington. Journal of Petrology 1975;16(2):272–313. doi:10.1093/petrology/16.2.272.

Früh-Green GL, Weissert H, Bernoulli D. A multiple fluid history recorded in Alpine ophiolites. Journal of the Geological Society 1990;147(6):959–70. doi:10.1144/gsjgs.147.6.0959.

Garuti G, Bartoli O, Scacchetti M, Zaccarini F. Volcanic massive sulfide deposits in the northern Apennines, Italy geological setting and structural styles of volcanic massive sulfide deposits in the northern Apennines (Italy): evidence for seafloor and sub-seafloor hydrothermal activity in unconventional ophiolites of the mesozoic Tethys. Boleten dela Sociedad Geolegica Mexicana 2008;60:121–45. doi:10.18268/BSGM2008v60n1a9.

Hannington M, Herzig P, Stoffers P, Scholten J, Botz R, Garbe-Schönberg D, Jonasson I, Roest W. First observations of high-temperature submarine hydrothermal vents and massive anhydrite deposits off the north coast of iceland. Marine Geology 2001;177(3-4):199–220.

Hess J, Bender ML, Schilling JG. Evolution of the ratio of strontium-87 to strontium-86 in seawater from cretaceous to present. Science 1986;231(4741):979–84.

Humphris SE, Klein F. Progress in deciphering the controls on the geochemistry of fluids in seafloor hydrothermal systems. Annual review of marine science 2018;10:315–43. doi:10.1146/annurev-marine-121916-063233.

Incerpi N, Martire L, Manatschal G, Bernasconi SM, Gerdes A, Czuppon G, Palcsu L, Karner GD, Johnson CA, Figueredo PH. Hydrothermal fluid flow associated to the extensional evolution of the adriatic rifted margin: Insights from the pre-to post-rift sedimentary sequence (se switzerland, n italy). Basin Research 2020;32(1):91–115. doi:10.1111/bre.12370.

Jackson JA. Active normal faulting and crustal extension. Geological Society, London, Special Publications 1987;28:3–17.

Jones CE, Jenkyns HC, Coe AL, Hesselbo SP. Quantification and restoration of extensional deformation along the Western Iberia and Newfoundland rifted margins. Geochimica et Cosmochimica Acta 1994;58(14):3061–74. doi:10.1016/0016-7037(94)90179-1.

Krasnov SG. Detailed geological studies of hydrothermal fields in the north atlantic. Geological Society, London, Special Publications 1995;87:43–64.

Le Gal V, Lucazeau F, Cannat M, Poort J, Monnin C, Battani A, Fontaine F, Goutorbe B, Rolandone F, Poitou C, et al. Heat flow, morphology, pore fluids and hydrothermal circulation in a typical Mid-Atlantic Ridge flank near oceanographer fracture zone. Earth and Planetary Science Letters 2018;482:423–33. doi:10.1016/j.epsl.2017.11.035.

Manatschal G, Müntener O. A type sequence across an ancient magma-poor ocean–continent transition: the example of the Western Alpine Tethys ophiolites. Tectonophysics 2009;473(1-2):4–19. doi:10.1016/j.tecto.2008.07.021.

Manatschal G, Nievergelt P. A continent-ocean transition recorded in the Err and Platta nappes (Eastern Switzerland). Eclogae Geologicae Helvetiae 1997;90(1):3–28. doi:10.5169/seals-168142.

McArthur J, Thirlwall M, Chen M, Gale A, Kennedy W. Strontium isotope stratigraphy in the late cretaceous: numerical calibration of the sr isotope curve and intercontinental correlation for the campanian. Paleoceanography 1993;8(6):859–73.

Mcculloch MT, Gregory RT, Wasserburg GJ, Taylor HP. A neodymium, strontium, and oxygen isotopic study of the cretaceous samail ophiolite and implications for the petrogenesis and seawater-hydrothermal alteration of oceanic crust. Earth and Planetarv Science Letters 1980;46:201.

McDonough W, McCulloch M, Sun S. Isotopic and geochemical systematics in tertiary-recent basalts from southeastern australia and implications for the evolution of the sub-continental lithosphere. Geochimica et Cosmochimica Acta 1985;49(10):2051–67. doi:10.1016/0016-7037(85)90063-8.

Melchert B, Devey CW, German C, Lackschewitz K, Seifert R, Walter M, Mertens C, Yoerger D, Baker E, Paulick H, et al. First evidence for high-temperature off-axis venting of deep crustal/mantle heat: The nibelungen hydrothermal field, southern mid-atlantic ridge. Earth and Planetary Science Letters 2008;275(1-2):61–9.

Mohn G, Manatschal G, Beltrando M, Masini E, Kusznir N. Necking of continental crust in magma-poor rifted margins: Evidence from the fossil alpine tethys margins. Tectonics 2012;31(1).

Müntener O, Manatschal G, Desmurs L, Pettke T. Plagioclase peridotites in ocean–continent transitions: refertilized mantle domains generated by melt stagnation in the shallow mantle lithosphere. Journal of Petrology 2010;51(1-2):255–94. doi:10.1093/petrology/egp087.

Müntener O, Pettke T, Desmurs L, Meier M, Schaltegger U. Refertilization of mantle peridotite in embryonic ocean basins: trace element and nd isotopic evidence and implications for crust–mantle relationships. Earth and Planetary Science Letters 2004;221(1-4):293–308. doi:10.1016/S0012-821X(04)00073-1.

Müntener O, Piccardo GB. Melt migration in ophiolitic peridotites: The message from Alpine-Apennine peridotites and implications for embryonic ocean basins. Geological Society Special Publication 2004;218:69–89. doi:10.1144/GSL.SP.2003.218.01.05.

Palandri JL, Reed MH. Geochemical models of metasomatism in ultramafic systems: serpentinization, rodingitization, and sea floor carbonate chimney precipitation. Geochimica et Cosmochimica Acta 2004;68(5):1115–33. doi:10.1016/j.gca.2003.08.006.

Panseri M, Fontana E, Tartarotti P. Evolution of rodingitic dykes: Metasomatism and metamorphism in the Mount Avic serpentinites (Alpine Ophiolites, southern Aosta Valley). Lithos 2008;33:165–85. doi:10.1016/j.lithos.2008.10.022.

Patten CG, Coltat R, Junge M, Peillod A, Ulrich M, Manatschal G, Kolb J. Ultramafic-hosted volcanogenic massive sulfide deposits: an overlooked subclass of vms deposit forming in complex tectonic environments. Earth-Science Reviews 2021;:103891.

Peltonen P, Kontinen A, Huhma H, Kuronen U. Outokumpu revisited: new mineral deposit model for the mantle peridotite-associated cu–co–zn–ni–ag–au sulphide deposits. Ore Geology Reviews 2008;33(3-4):559–617.

Perseil EA, Latouche L. Decouverte de microstructures de nodules polymetalliques dans les mineralisations manganesiferes metamorphiques de falotta et de parsettens (grisons-suisse). Mineral Deposita 1989;24:111–6. doi:10.1007/bf00206312.

Picazo S, Manatschal G, Cannat M, Andréani M. Deformation associated to exhumation of serpentinized mantle rocks in a fossil ocean continent transition: The totalp unit in se switzerland. Lithos 2013;175:255–71. doi:10.1016/j.lithos.2013.05.010.

Picazo S, Müntener O, Manatschal G, Bauville A, Karner G, Johnson C. Mapping the nature of mantle domains in western and central europe based on clinopyroxene and spinel chemistry: Evidence for mantle modification during an extensional cycle. Lithos 2016;266:233–63.

Pin C, Zaldueguil JFS. Sequential separation of light rare-earth elements, thorium and uranium by miniaturized extraction chromatography: Application to isotopic analyses of silicate rocks. Analytica Chimica Acta 1997;339:79–89. doi:10.1016/S0003-2670(96)00499-0.

Rampone E, Hofmann AW, Raczek I. Isotopic contrasts within the internal liguride ophiolite (n. italy): the lack of a genetic mantle-crust link. Earth and Planetary Science Letters 1998;163:175–89. doi:10.1016/S0012-821X(98)00185-X.

Rona PA. Hydrothermal activity at the trans-atlantic geotraverse hydrothermal field, Mid-Atlantic Ridge crest at 26°N. Journal of Geophysical Research 1984;89:11365–77. doi:10.1029/JB089iB13p11365.

Rona PA, Hannington MD, Raman C, Thompson G, Tivey MK, Humphris SE, Lalou C, Petersen S. Active and relict sea-floor hydrothermal mineralization at the TAG hydrothermal field, Mid-Atlantic Ridge. Economic Geology 1993;88(8):1989–2017. doi:10.2113/gsecongeo.88.8.1989.

Rouxel O, Fouquet Y, Ludden JN. Copper isotope systematics of the lucky strike, rainbow, and logatchev sea-floor hydrothermal fields on the Mid-Atlantic Ridge. Economic Geology 2004a;99:585–600. doi:10.1016/j.chemgeo.2005.04.011.

Rouxel O, Fouquet Y, Ludden JN. Subsurface processes at the lucky strike hydrothermal field, Mid-Atlantic Ridge: Evidence from sulfur, selenium, and iron isotopes. Geochimica et Cosmochimica Acta 2004b;68:2295–311. doi:10.1016/j.gca.2003.11.029.

Salvioli-Mariani E, Boschetti T, Toscani L, Montanini A, Petriglieri JR, Bersani D. Multi-stage rodingitization of ophiolitic bodies from northern apennines (italy): Constraints from petrography, geochemistry and thermodynamic modelling. Geoscience Frontiers 2020;11(6):2103–25. doi:10.1016/j.gsf.2020.04.017.

Schaltegger U, Desmurs L, Manatschal G, Müntener O, Meier M, Frank M, Bernoulli D. The transition from rifting to sea-floor spreading within a magma-poor rifted margin: Field and isotopic constraints. Terra Nova 2002;14(3):156–62. doi:10.1046/j.1365-3121.2002.00406.x.

Schwarzenbach EM, Vogel M, Früh-Green GL, Boschi C. Serpentinization, carbonation, and metasomatism of ultramafic sequences in the Northern Apennine Ophiolite (nw italy). Journal of Geophysical Research: Solid Earth 2021;126. doi:10.1029/2020jb020619.

Seyfried Jr W, Foustoukos D, Allen D. Ultramafic-hosted hydrothermal systems at mid-ocean ridges: Chemical and physical controls on ph, redox and carbon reduction reactions. Mid-Ocean Ridges: Hydrothermal Interactions Between the Lithosphere and Oceans 2004;148:267–84. doi:10.1029/148GM11.

Seyfried Jr W, Pester NJ, Tutolo BM, Ding K. The Lost City hydrothermal system: Constraints imposed by vent fluid chemistry and reaction path models on subseafloor heat and mass transfer processes. Geochimica et Cosmochimica Acta 2015;163:59–79. doi:10.1016/j.gca.2015.04.040.

Spooner E, Beckinsale R, Fyfe W, Smewing J. O18 enriched ophiolitic metabasic rocks from e. liguria (italy), pindos (greece), and troodos (cyprus). Contributions to Mineralogy and Petrology 1974;47(1):41–62.

Stille P, Clauer N, Abrech J. Nd isotopic composition of jurassic Tethys seawater and the genesis of Alpine mn-deposits: Evidence from sr-nd isotope data. Geochemica et Cosmochimica 1989;53:1095–9. doi:10.1016/0016-7037(89)90214-7.

Tao C, Li H, Jin X, Zhou J, Wu T, He Y, Deng X, Gu C, Zhang G, Liu W. Seafloor hydrothermal activity and polymetallic sulfide exploration on the southwest indian ridge. Chinese Science Bulletin 2014;59(19):2266–76. doi:10.3390/min10110970.

Tao C, Seyfried W, Lowell R, Liu Y, Liang J, Guo Z, Ding K, Zhang H, Liu J, Qiu L, et al. Deep high-temperature hydrothermal circulation in a detachment faulting system on the ultra-slow spreading ridge. Nature communications 2020;11(1):1–9. doi:10.1038/s41467-020-15062-w.

Toffolo L, Nimis P, Martin S, Tumiati S, Bach W. The Cogne magnetite deposit (Western Alps, italy): A late jurassic seafloor ultramafic-hosted hydrothermal system? Ore Geology Reviews 2017;83:103–26. doi:10.1016/j.oregeorev.2016.11.030.

Veizer J, Ala D, Azmy K, Bruckschen P, Buhl D, Bruhn F, Carden GA, Diener A, Ebneth S, Godderis Y, et al. 87sr/86sr, δ13c and δ18o evolution of phanerozoic seawater. Chemical geology 1999;161(1-3):59–88.

Veizer J, Compston W. 87sr/86sr composition of seawater during the phanerozoic. Geochimica et Cosmochimica Acta 1974;38. doi:10.1016/0016-7037(74)90099-4.

Viti C, Mellini M. Mesh textures and bastites in the elba retrograde serpentinites. Eur J Mineral 1998;10:1341–59. doi:10.1127/ejm/10/6/1341.

Von Damm KL. Controls on the chemistry and temporal variability of seafloor hydrothermal fluids. Seafloor hydrothermal systems: Physical, chemical, biological, and geological interactions 1995;91:222–47. doi:10.1029/GM091p0222.

Weissert H, Bernoulli D. Oxygen isotope composition of calcite in Alpine ophicarbonates: a hydrothermal or Alpine metamorphic signal? Eclogae Geologicae Helvetiae 1984;77(1):29–43. doi:10.5169/seals-165497.

Willbold M, Andreas S. Formation of enriched mantle components by recycling of upper and lower continental crust. Chemical Geology 2010;276(3-4):188–97. doi:10.1016/j.chemgeo.2010.06.005.

Wolery TJ, Sleep NH. Hydrothermal circulation and geochemical flux at mid-ocean ridges. The Journal of Geology 1976;84(3):249–75. doi:10.1086/628195.

Zeng Z, Ma Y, Chen S, Selby D, Wang X, Yin X. Sulfur and lead isotopic compositions of massive sulfides from deep-sea hydrothermal systems: Implications for ore genesis and fluid circulation. Ore Geology Reviews 2017;87:155–71. doi:10.1016/j.oregeorev.2016.10.014.

Zhu X, Guo Y, Williams R, Onions R, Matthews A, Belshaw N, Canters G, De Waal E, Weser U, Burgess B, et al. Mass fractionation processes of transition metal isotopes. Earth and Planetary Science Letters 2002;200(1-2):47–62. doi:10.1016/S0012-821X(02)00615-5.

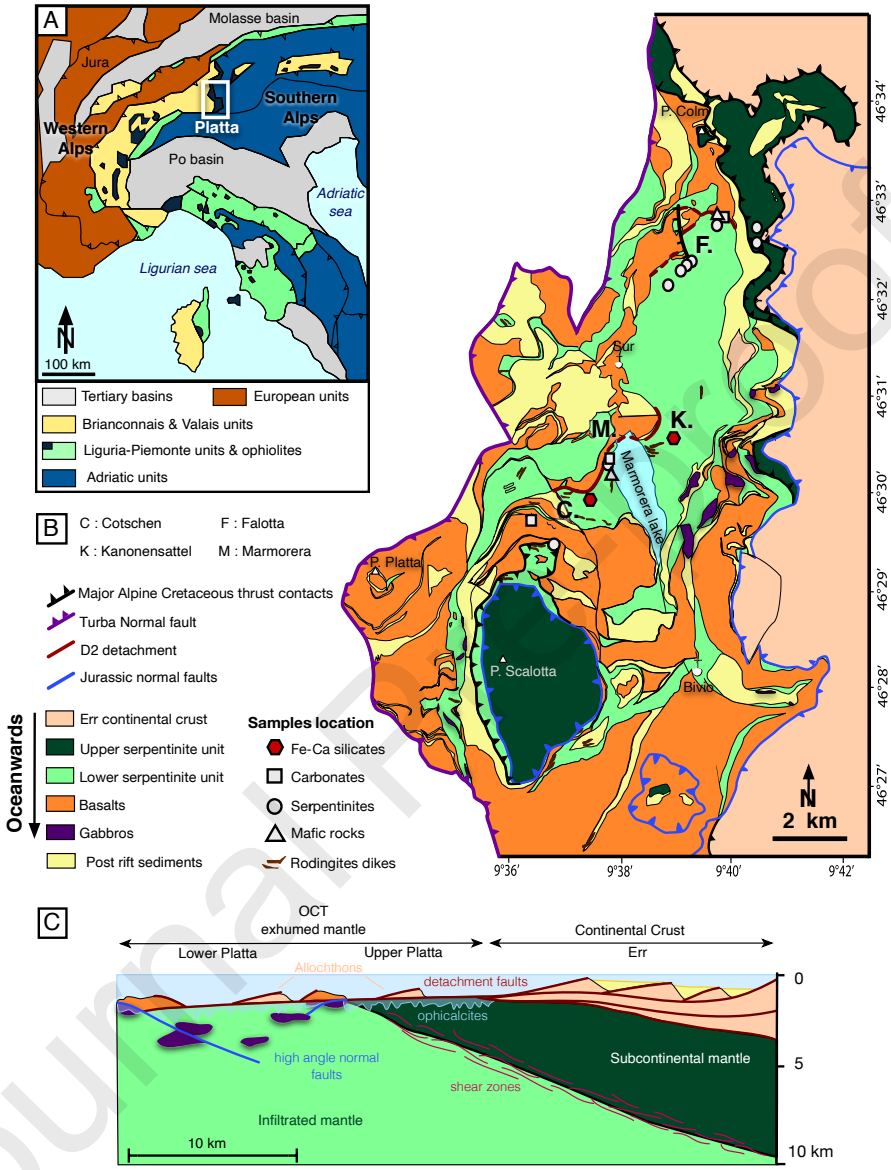

Figure 1: A) Simplified map of the major paleogeographic units of the Western and Central Alps and the Apennines, with location of the study area (white frame) modified after Manatschal and Müntener (2009). B) Geological map of the Platta nappe with samples location (modified after Schaltegger et al. (2002)). C) Distribution of subcontinental and infiltrated mantle domains along an ocean-continent-transition of the former Alpine Tethys (modified after Müntener and Piccardo (2004)).

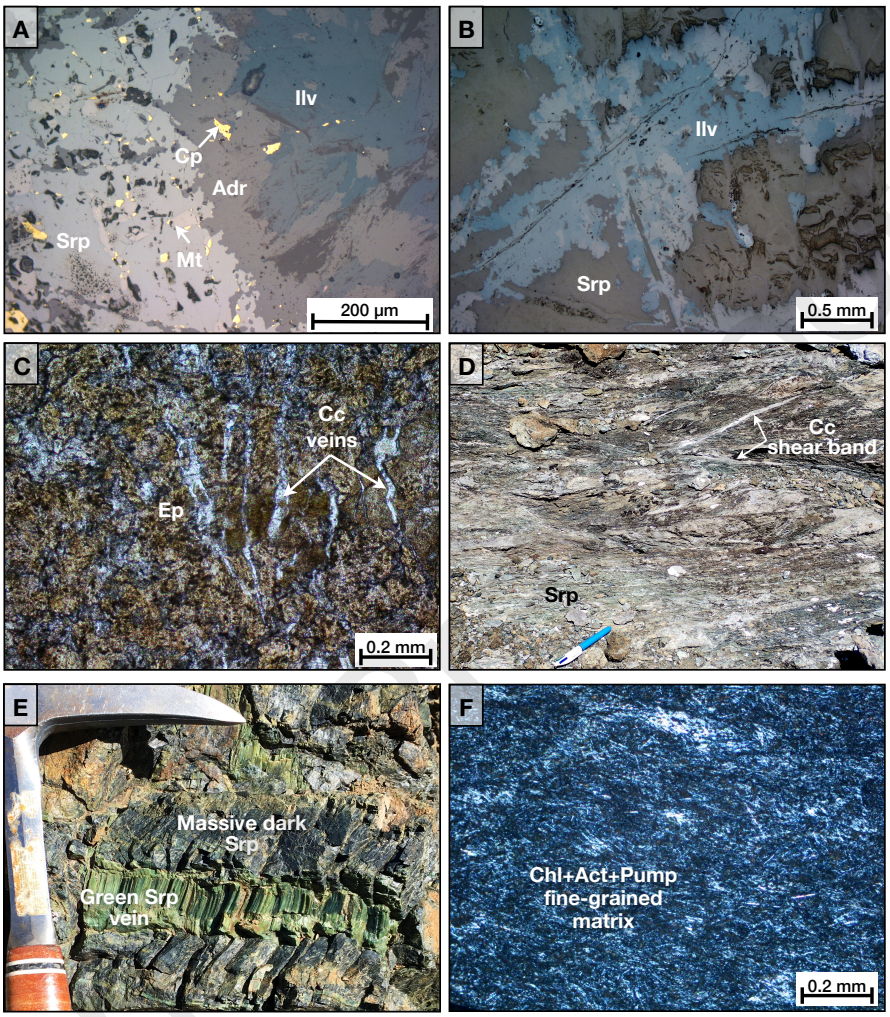

Figure 2: Representative macroscopic and microscopic pictures illustrating the different lithologies reported in the Platta nappe (Cotschen and Falotta sites). A) Fe-Ca silicates (ilvaite and andradite) associated with sulfides (sphalerite, chalcopyrite) and oxides (magnetite (Mt) pervasively replacing serpentinite. B) Fe-Ca silicate (ilvaite) in veins (stockwork structure) cutting through serpentinite. C) Discrete calcite veins crosscutting an epidotized basalt. D) Calcite shear band cutting through serpentinite. E) Green serpentine vein crosscutting a massive dark serpentine. F) Basalt altered to an assemblage made of chlorite, actinolite and pumpellyite. Chl=chlorite; Act=actinolite; Pump=pumpellyite; Ilv=ilvaite; Adr=(hydro)andradite; Srp=serpentine; Mt=magnetite; Sph=sphalerite; Cp=chalcopyrite; Cc=calcite

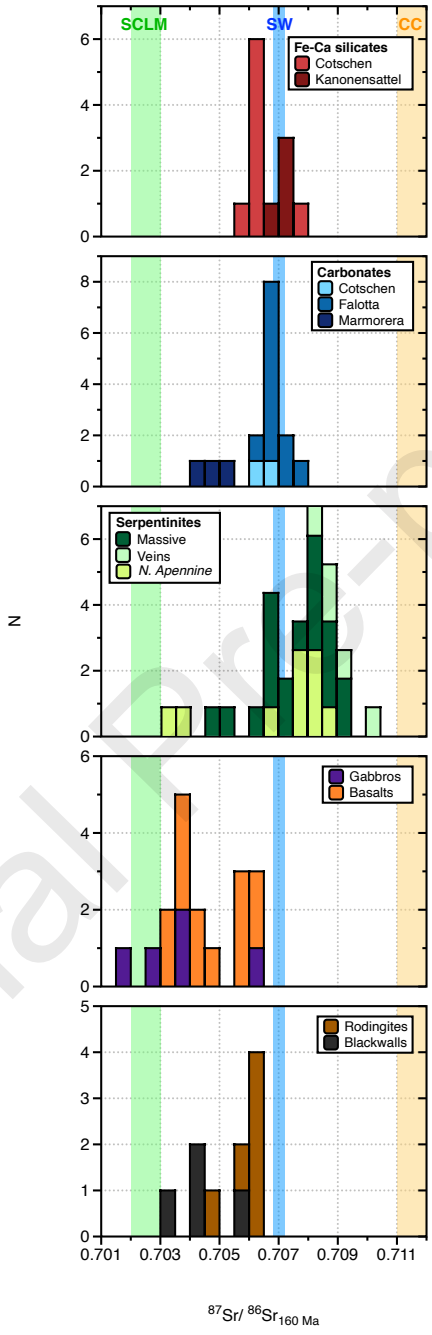

Figure 3: Histograms of $^{87}Sr/^{86}Sr$ recalculated at 160 Ma for the different lithologies. SCLM: Sub Continental Lithospheric Mantle from McDonough et al. (1985), SW: Seawater from Jones et al. (1994) and CC: Continental Crust values from Willbold and Andreas (2010). N. Apennine serpentinites from Schwarzenbach et al. (2021).

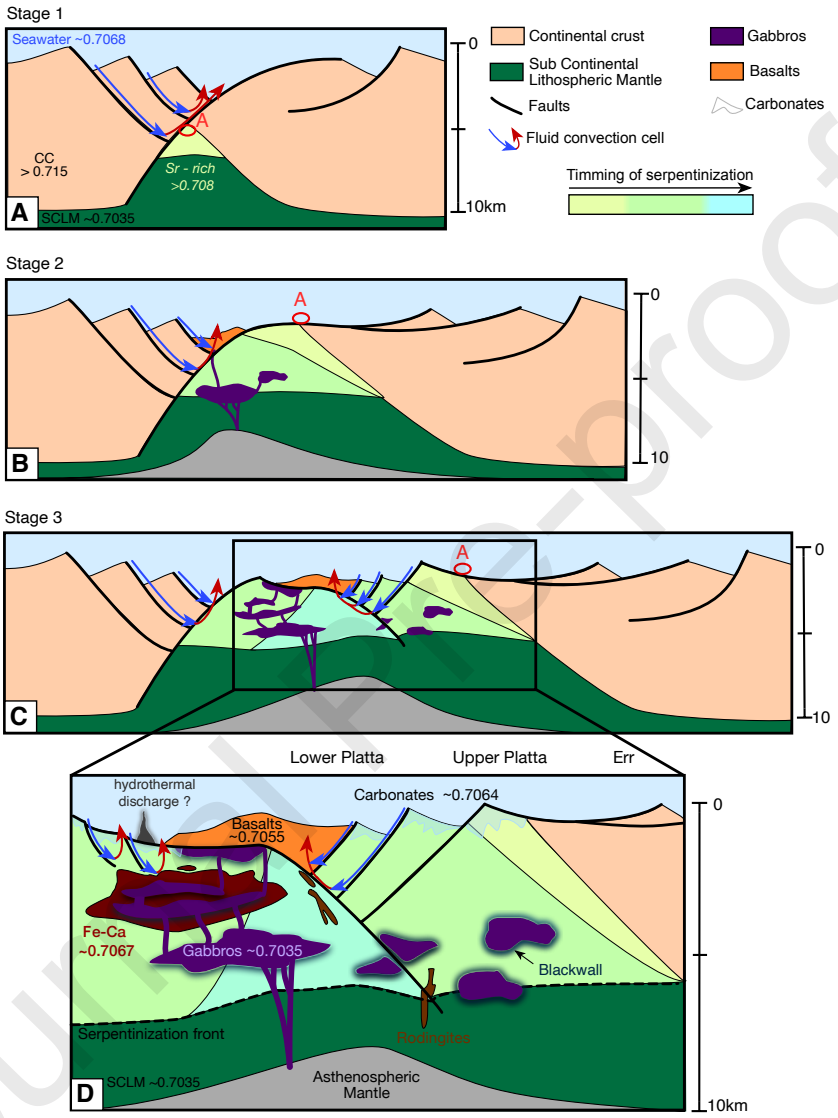

Figure 4: Schematic model showing the evolution of the OCT and associated fluid circulations leading to the formation of Fe-Ca silicates, modified from Epin et al. (2019). A) Stage 1: serpentinization initiated from fluids with radiogenic Sr (CC-derived fluids) leading to formation of serpentinites with Sr isotope compositions higher than SW. B) Stage 2: first exhumation of subcontinental lithospheric mantle previously serpentinized and onset of magmatism, serpentinization continues to occur by seawater with a lesser continental influence. C) Stage 3: increase of magmatic rocks and alteration (rodingitization, epidotization-chloritization of mafic extrusives) by serpentinization derived fluids mixing with seawater infiltrated along faults. Serpentinization continues to occur with pristine seawater. D) Schematic model showing fluids pathways, the different alteration products and their associated Sr isotope compositions. Fluids resulting from the alteration of mafic rocks and serpentinization migrated upwards and mixed with seawater to form Fe-Ca silicates. Carbonation was the last hydrothermal event recording in ultramafic and mafic rocks.

Table 1: Sr isotope compositions of Fe-Ca silicates, serpentinites, carbonates and mafic rocks sampled in the Platta nappe 87Sr/86Sr in it

Site	Sample	Latitude	Longitude	$^{87}Sr/^{86}Sr_{mes}$	2 SE	$^{87}Sr/^{86}Sr_{160\ Ma}$	Sr ppm	Rb ppm	Sr exchange (%)
						Fe-Ca-silicates			
Cotschen	Cot18_40	46°29'56N	9°37'16E	0.706462	0.000010	*0.70646*			87
	Cot18_46	46°29'56N	9°37'16E	0.707848	0.000012	*0.70785*			*nd*
	Cot18_50	46°29'56N	9°37'16E	0.706456	0.000013	*0.70646*			87
	Cot18_57	46°29'55N	9°36'55E	0.70592	0.000022	*0.70592*			75
	Cot18_66	46°29'54N	9°36'58E	0.706325	0.000010	*0.70633*			84
	Cot18_67	46°29'54N	9°36'58E	0.706419	0.000011	*0.70642*			86
	Cot18_70	46°29'54N	9°36'58E	0.706422	0.000015	*0.70642*			86
	Cot18_72	46°29'54N	9°36'58E	0.706027	0.000013	*0.70603*			77
Kanonensatel	Kan19_3	46°30'48N	9°38'35E	0.707114	0.000029	*0.70711*			*nd*
	Kan19_5	46°30'48N	9°38'35E	0.707456	0.000010	*0.70746*			*nd*
	Kan19_7	46°30'48N	9°38'35E	0.707045	0.000013	*0.70705*			100
	Kan19_9	46°30'48N	9°38'35E	0.706708	0.000013	*0.70671*			93
						Carbonates			
Cotschen	Cot16_49a	46°30'02 N	9°36'42E	0.706588	0.000010	*0.70659*			*90*
	Cot16_52	46°30'02 N	9°36'42E	0.706311	0.000010	*0.70631*			*84*
Marmorera	Mar16_37	46°30'18 N	9°37'40E	0.704193	0.000010	*0.70419*			*36*
	Mar16_40a	46°30'18 N	9°37'40E	0.705481	0.000010	*0.70548*			*65*
	Mar16_40e	46°30'18 N	9°37'40E	0.704675	0.000010	*0.70468*			*46*
Falotta	Fal16_16	46°32'42N	9°39'36E	0.707294	0.000010	*0.70729*			*nd*
	Fal16_17	46°32'42N	9°39'36E	0.706677	0.000010	*0.70668*			*92*
	Fal17_28	46°32'42N	9°39'36E	0.707220	0.000010	*0.70722*			*nd*
	Fal17_63	46°32'42N	9°39'36E	0.706866	0.000010	*0.70687*			*96*
	Fal17_64	46°32'42N	9°39'36E	0.706835	0.000010	*0.70684*			*95*
	Fal17_65	46°32'42N	9°39'36E	0.706868	0.000010	*0.70687*			*96*
	Fal17_35	46°32'42N	9°39'36E	0.706813	0.000010	*0.70681*			*95*
	Fal17_42	46°32'42N	9°39'36E	0.706731	0.000010	*0.70673*			*93*
	Fal17_49b	46°32'42N	9°39'36E	0.706418	0.000010	*0.70642*			*86*
	Fal17_51	46°32'42N	9°39'36E	0.706657	0.000010	*0.70666*			*91*
						Serpentinites			
Cotschen	Tal-18-01	46°29'43N	9°37'21E	0.707668	0.000018	0.706826	0.55	0.07	95
	Tal-18-06a	46°29'43N	9°37'19E	0.709049	0.000025	0.707798	0.42	0.08	*nd*
Marmorera	Mar 18-01	46°30'20N	9°37'41E	0.704621	0.000040	0.703939	4.40	0.59	30
Kanonensatel	KAN-19-10	46°30'48N	9°38'35E	0.707677	0.000013	0.706885	12.8	1.54	97
Falotta LP	Fal17_18	46°32'51N	9°39'9E	0.708068	0.000015	0.708068	1.12	0.00	*nd*
	Fal17_20	46°32'51N	9°39'9E	0.708075	0.000010	0.708075	1.14	0.00	*nd*
	Fal17_22	46°32'51N	9°39'9E	0.709308	0.000010	0.708580	5.55	0.62	*nd*
	Fal17_23	46°32'51N	9°39'9E	0.709408	0.000010	0.708134	1.13	0.22	*nd*
	Fal 18-11	46°32'44N	9°39'39E	0.706826	0.000009	0.706303	1.50	0.12	83
	Fal 18-12	46°32'43N	9°39'34E	0.706754	0.000006	0.706481	13.5	0.58	87
	Fal 18-13	46°32'42N	9°39'35E	0.707383	0.000004	0.705745	5.00	1.24	71
	Fal 18-14	46°32'30N	9°39'40E	0.708211	0.000006	0.706755	2.00	0.44	94
	TG-P-1a	46°32'51N	9°39'9E	0.707431	0.000010	0.707431			*nd*
	TG-P-1b	46°32'51N	9°39'9E	0.708495	0.000010	0.708495			*nd*
Falotta UP	Fal 18-02a	46°32'51N	9°40'10E	0.709274	0.000009	0.708432	0.70	0.09	*nd*

	Fal 18-02b	46°32'51N	9°40'10E	0.709006	0.000009	0.708579	2.40	0.17	*nd*
	Fal 18-03	46°32'51N	9°40'10E	0.708520	0.000003	0.708122	6.10	0.39	*nd*
	Fal 18-04	46°32'51N	9°40'10E	0.710033	0.000006	0.708752	0.90	0.18	*nd*
	Fal 18-05	46°32'51N	9°40'10E	0.708889	0.000011	0.707704	0.50	0.09	*nd*
	Fal 18-06	46°32'51N	9°40'10E	0.708954	0.000010	0.708226	4.10	0.45	*nd*
	Fal 18-07	46°32'51N	9°40'10E	0.705323	0.000010	0.704852	13.4	0.96	51
	Fal 18-08	46°32'57N	9°40'7E	0.708644	0.000015	0.708144	1.60	0.12	*nd*
	Fal 18-09	46°32'57N	9°40'7E	0.709482	0.000003	0.709391	3.50	0.55	*nd*
	Fal 18-10	46°32'57N	9°40'7E	0.706453	0.000004	0.706135	1.40	0.07	80
							Mafic rocks		
Marmorera	A	46°30'22N	9°37'39E	0.704651	0.000009	0.704628	393	0.76	45
	D	46°30'22N	9°37'39E	0.704638	0.000010	0.704342	1240	56.6	39
	Mar18_17	46°30'18N	9°37'40E	0.703860	0.000010	0.703337	37.4	0.60	16
	Mar18_28	46°30'18N	9°37'40E	0.703781	0.000010	0.70369	80.6	1.20	24
Falotta LP	Fal17_38	46°32'42N	9°39'36E	0.706243	0.000010	0.706243	3.94	0.00	82
	Fal17_39	46°32'42N	9°39'36E	0.705879	0.000010	0.705879	3.68	0.00	74
	Fal17_44	46°32'42N	9°39'36E	0.706071	0.000010	0.706026	1840	13.1	77
	Fal17_49a	46°32'42N	9°39'36E	0.705990	0.000009	0.705967	4790	16.1	76

alics refers 87Sr/86Sr(mes) without Rb correction.

W/R closed system	W/R open system	Comment
nd	*nd*	pervasive replacement
nd	*nd*	pervasive replacement
nd	*nd*	veins in serpentinite
nd	*nd*	veins in serpentinite
nd	*nd*	pervasive replacement
nd	*nd*	veins in serpentinite
nd	*nd*	pervasive replacement
nd	*nd*	veins in serpentinite
nd	*nd*	pervasive replacement
nd	*nd*	pervasive replacement
nd	*nd*	pervasive replacement
nd	*nd*	pervasive replacement
nd	*nd*	veins in serpentinite
nd	*nd*	veins in serpentinite
nd	*nd*	veins in serpentinite
nd	*nd*	veins in serpentinite
nd	*nd*	pervasive replacement in serpentinite
nd	*nd*	discret veins in serpentinite
nd	*nd*	discret veins in serpentinite
nd	*nd*	discret veins in serpentinite
nd	*nd*	pervasive replacement in serpentinite
nd	*nd*	pervasive replacement in serpentinite
nd	*nd*	pervasive replacement in serpentinite
nd	*nd*	veins in epidotized basalt
`*nd*	*nd*	veins in epidotized basalt
nd	*nd*	veins in epidotized basalt
nd	*nd*	veins in epidotized basalt
16.0	2.4	
nd	nd	
0.5	0.4	
35	4.2	
nd	*nd*	
nd	*nd*	
nd	*nd*	veins
nd	*nd*	veins
6.3	2.3	
8.7	2.6	
3.0	1.5	
18.3	3.4	
nd	*nd*	
nd	*nd*	
nd	*nd*	veins

nd	*nd*	
nd	*nd*	
nd	*nd*	veins
nd	*nd*	veins
nd	*nd*	
1.3	*0.9*	
nd	*nd*	
nd	*nd*	
nd	*nd*	
1.0	0.8	epidotized basalt
0.8	0.6	epidotized basalt
0.2	0.2	mafic intrusion
0.4	0.3	mafic intrusion (mineralized)
5.7	2.2	chloritized basalt
3.5	1.7	nodule of chloritized basalt
4.2	1.8	epidotized basalt
3.9	1.8	epidotized basalt